Al_nBi Clusters: Transitions Between Aromatic and Jellium Stability

Charles E. Jones, Jr.,[†] Peneé A. Clayborne,[‡] J. Ulises Reveles,[‡] Joshua J. Melko,[†] Ujjwal Gupta,[†] Shiv N. Khanna,[‡] and A. W. Castleman, Jr.*[,†]

Departments of Chemistry and Physics, The Pennsylvania State University, University Park, Pennsylvania 16802, and Department of Physics, Virginia Commonwealth University, Richmond, Virginia 23284

Received: May 27, 2008; Revised Manuscript Received: October 15, 2008

An experimental and theoretical study of bismuth-doped aluminum clusters in the gas phase has revealed two particularly stable clusters, namely, Al_3Bi and Al_5Bi. We show that their electronic structure can be understood in terms of the aromatic and “Jellium” models, respectively. Negative ion photodetachment spectra provide a fingerprint of the electronic states in Al_nBi^- ($n = 1-5$) anions, while theoretical investigations reveal the nature of the electronic orbitals involved. Together, the findings reveal that the all-metal Al_3Bi cluster with 14 valence electrons is a cyclic, planar structure with a calculated large ionization potential of 7.08 eV, a low electron affinity of 1.41 eV, and a large gap of 1.69 eV between the highest occupied and lowest unoccupied molecular orbitals (HOMO−LUMO gap). The Al_3Bi cluster has molecular orbitals reminiscent of aromatic systems and is a neutral cluster with no need for counterion or ligand support. A slightly larger cluster, Al_5Bi, has 20 valence electrons and is another highly stable compact structure with a calculated large ionization potential of 6.51 eV and a large HOMO−LUMO gap of 1.15 eV. This cluster’s stability is rooted in a Jellium electronic shell closing. The formation of stable species using aromatic bonding allows us to extend the idea of cluster-assembled materials built out of stable clusters with Jellium shell closings (superatoms) to include ones involving aromatic building blocks.

1. Introduction

The electronic structure and the chemical behavior of small metal clusters can be fundamentally different from the bulk, where the electronic states are well described by band theory. Metal clusters, which feature both finite size and structural flexibility, inherently have a unique relationship between geometry and electronic states. When the structure and electronic states are manipulated, the stability and chemical characteristics can be tuned through ways that are generally inaccessible in the bulk phase.[1−3] For clusters of free-electron metals, a model is commonly used in which the nuclei and innermost electrons form a positively charged core with an essentially uniform potential. Valence electrons from individual atoms in the cluster are then subjected to this uniform potential, and a Jellium electronic shell structure emerges with stable numbers in electron configurations (2, 8, 18, 20, ...) that differ from either the atomic series (2, 10, 18, ...) or the bulk system.[4] This model accounts for the stability of numerous simple and compound metal clusters with electron counts leading to closed electronic shells. In aluminum clusters, which have three valence electrons per atom, this model explains the observed stability and chemical inertness of Al_{13}^-, which contains 40 valence electrons. The model also explains the high electron affinity of Al_{13}, with 39 valence electrons, because the highest occupied molecular orbital (HOMO) needs one p-like electron to complete its shell.[5] We have previously demonstrated, both experimentally and theoretically, the superhalogen character of Al_{13} in anionic species formed by combining it with a halogen atom,[6] and our current investigations are focused on identifying particular clusters that display enhanced stability.[7]

A different concept to explain electronic stabilization, aromaticity, has been applied to organic systems for over a century[8,9] as a way to describe stable molecules with delocalized bonding. Organic molecules that are conjugated, cyclic, and planar and that contain $(4n + 2)\pi$ electrons are traditionally classified as aromatic. Recent studies by Li et al. have extended aromaticity to include all-metal anionic molecules, most notably the Al_4^{2-} dianion.[10] An experimental and theoretical examination of MAl_4^- (M = Li, Na, or Cu) clusters provided evidence that Al_4^{2-} favors a cyclic, planar structure with two delocalized π electrons. Further studies revealed that the extent of delocalization in Al_4^{2-} includes σ electrons as well, accounting for its threefold aromaticity (one pair of π electrons and two pairs of σ electrons). Boldyrev and Kuznetsov calculated resonance energies for all-metal aromatic systems[11] and found unusually high values of 48 kcal/mol for Na_2Al_4 and 21 kcal/mol for Na_2Ga_4 (compared to 20 kcal/mol in benzene, the most well-known aromatic molecule). Previous experimental studies of all-metal aromatic clusters investigated species that are isoelectronic with Al_4^{2-}, including X_4^{2-} where X is B, Ga, In, or Tl,[12] mixed valence isoelectronic species MAl_3^-, where M is Si, Ge, Sn, or Pb,[13] and triatomic aromatics of the form X_3^-, where X is B, Al, or Ga.[14,15] Additionally, studies on similar mixed systems, including theoretical work on Al_3As and experiments involving Al_3P, have also been reported.[16,17] Recent reviews of all-metal aromaticity written by Boldyrev et al. provide a comprehensive guide to work reported in the literature.[18]

The above examples of Jellium and aromatic clusters show that, depending on the electron count and the number of atoms, the electron gas has the potential to stabilize clusters through different mechanisms. Clusters with 2, 8, 18, 20, ... valence electrons favor a compact geometry and lead to stability via a Jellium-like model, whereas clusters with $(4n + 2)\pi$ electrons favor a planar arrangement and aromatic stability. It would be

---

* To whom correspondence should be addressed. E-mail: awc@psu.edu.
[†] The Pennsylvania State University.
[‡] Virginia Commonwealth University.

10.1021/jp804667d CCC: $40.75

ideal to find a system where the electron count could be varied to fit either of the two scenarios and then to demonstrate how the geometrical arrangements and the electronic states in the same system adapt for stabilization. In the present work, we demonstrate this unusual possibility in Al_n clusters doped with a single Bi atom. The valence electron configuration of Al is $3s^23p^1$ and that of Bi is $6s^26p^3$. Pure aluminum clusters are known to undergo a transition from a monovalent to a trivalent state in small sizes.[19] Depending on the contributions of s and p electrons, Al_3Bi would correspond to either a six p-electron system in a planar configuration or a 14 valence electron cluster with a compact structure that favors s−p mixing. A valence configuration of 6 makes it isoelectronic with Al_4^{2-} with six p-electrons that exhibit aromatic bonding. This may imply that Al_3Bi should have a planar structure and enhanced energetic stability.

If the stability of Al_3Bi is caused by the combination of p-electrons in a planar structure, then naturally the addition or removal of one electron would cause destabilization and geometric distortion. For example, adding one electron to the neutral Al_3Bi cluster to form Al_3Bi^- (seven p-electrons, 15 total) should reduce the stability of the planar geometry relative to the compact geometry. The Al_3Bi^- cluster, with a nonplanar, more compact structure, will also have a smaller HOMO−LUMO gap indicative of lower chemical stability. With negative ion photodetachment spectra, where the peaks in the photoelectron spectrum sample the valence electronic states of the neutral cluster in the anionic ground-state geometry, this structural transition can be directly probed. The addition of two electrons, however, to Al_3Bi would make an Al_3Bi^{2-} cluster with eight p- and 16 total electrons favoring a compact geometry if the Coulomb repulsion between the extra two electrons could be eliminated. We demonstrate theoretically that the addition of electrons to an aromatic bonding scheme causes the molecular orbitals to become reminiscent of a Jellium scheme. This is performed to describe the interplay between aromaticity and the Jellium model in understanding bonding in metal clusters.

In Al_5Bi, another potential Jellium situation arises. Each Al contributes three valence electrons, while Bi contributes five valence electrons. The cluster therefore contains a total of 20 valence electrons corresponding to a closed Jellium shell, and it would be expected to have a symmetric and compact three-dimensional geometry with a large HOMO−LUMO gap. This shows that, with the right geometry and electron count, both aromaticity and Jellium closings can be achieved for many permutations of metals and nonmetals in the periodic table. In both types of stability, the valence electrons of individual atoms in a given cluster combine for cooperative bonding effects. Aluminum clusters doped with bismuth atoms are thus an ideal system in which the interplay between aromaticity and Jellium stability can be observed.

In this work, we carry out a synergistic effort combining experimental data with first principles electronic structure studies to demonstrate these two differing facets of the electron gas. For the experimental component, we use negative ion photodetachment spectroscopy as a probe of the electronic states. A comparison between the experimental photoelectron spectra and the calculated spectra of anions provides a fingerprint of the neutral electronic states with the caveat that the neutral species are probed in the anionic geometry. The experimentally observed species are then examined theoretically with established "pointers" that prove both energetic stability and chemical hardness. Energetic stability is demonstrated by a large energy gain when a cluster forms from a stoichiometry with one less atom and by a small energy gain when one additional atom binds to the cluster. Chemical hardness is the resistance to change in electron number or deformation of the electron cloud and is tested by the size of the HOMO−LUMO gap as a large gap indicates inertness. Both the experimental and computational parts of the present study are essential for a complete picture of the clusters investigated.

We had previously proposed that selected clusters exhibiting Jellium stability could be described as "superatoms" asserting that clusters of a given element can have chemical and electronic properties resembling those of another atom in the periodic table.[6,20] A new type of chemistry, one involving clusters taking on the role of atoms as the basic building blocks, is already possible. The ability to identify and synthesize inert clusters using aromaticity allows us to have even more building blocks at our disposal in the creation of cluster-assembled materials. In the next section, we describe our experimental and computational methods. Results and discussion are then given in section 3. Final conclusions are drawn in the last section.

2. Experimental and Computational Methods

Experiments were performed with a magnetic bottle photoelectron spectroscopy apparatus that has been described in detail previously.[21] A laser vaporization supersonic cluster beam source synthesizes anionic clusters of interest. Two methods were successful in creating Al_nBi^- clusters. The first made use of two adjacent rods of pure aluminum and bismuth that met at the laser's focal point. A second method used a thin layer of bismuth coated on an aluminum rod. In both cases, helium was used as the carrier gas with stagnation pressures between 50 and 75 psi. Negative ions were extracted and mass analyzed with a Wiley−McLaren time-of-flight mass spectrometer.[22] Mass-selected anions of interest were interrogated by a laser beam from an unpolarized XeCl excimer laser (308 nm) in a magnetic bottle time-of-flight electron analyzer, where photodetached electrons were detected according to their kinetic energies. The resolution of our apparatus was estimated to be better than 300 meV at a binding energy of 1 eV. Electronic spectra were calibrated on the basis of the known spectra of Bi^-.[23]

First principles electronic structure studies on the anionic, neutral, and cationic forms of Al_nBi ($n = 1-6$) clusters were performed within the density functional formalism[24] employing the Perdew, Burke, and Enzerhof (PBE96)[25] generalized gradient approximation. The actual calculations were carried out using the deMon2k software.[26] The electronic orbitals and eigenstates were determined by using a linear combination of Gaussian atomic type orbitals molecular orbital approach. For Al, we employed the density functional theory (DFT) optimized DZVP basis set,[27] and the Bi atom was described using the 23 electron scalar relativistic effective core potential proposed by Metz et al.[28] in combination with the correlation consistent aug-cc-pVDZ valence basis set.[29] To avoid the calculation of four-center electron repulsion integrals, a variational fitting of the Coulomb potential was employed.[30,31] The auxiliary density was expanded in primitive Hermite Gaussian functions using the GEN-A2 auxiliary function set that contains s, p, and d functions for Al and the GEN-A2* auxiliary function set with similar structure as the GEN-A2 set but also including f and g functions for Bi. The exchange-correlation potential was calculated with the orbital density. The numerical integration of the exchange-correlation energy and potential was performed on an adaptive grid,[32] and a half-numeric integrator was employed for the effective core potential (ECP) integrals.[33] To determine the ground-state geometries, the configuration space was sampled by starting from several initial configurations and spin states. All the structures were fully optimized in redundant coordinates without symmetry constraints,[34] and resulting ground states were ascertained via a frequency analysis.

The methodology was first tested via studies on pure neutral and anionic aluminum clusters Al_n with $n = 1-6$. The geometries and ground-state spin multiplicities of these clusters have been previously investigated by Sun et al.[35] with the B3LYP/6−311G(2d) model and by Zhan et al.[36] ($n = 1-4$) at the high-level CCSD(T)/aug-ccPVxZ (x = D, T, and Q); our results agree with those investigations. The calculated adiabatic, and vertical, detachment energies (ADE, VDE) for the Al_n^- series ($n = 2-6$) showed very good agreement (deviations of less than 0.1 eV, Supplemental Tables S1 and S2) with respect to the theoretical results of Sun et al.[35] and of Zhan et al.[36] and with the experimental values reported by Li et al.[19] and by Cha et al.[37] The only exception was Al_3^- for which our calculated ADE of 1.64 eV underestimated the experimental value of 1.90 ± 0.1 eV.[19,37] Interestingly, Zhan et al.[36] predicted an ADE of 1.89 eV in excellent agreement with the experimental value. To further investigate this difference, we compared our optimized Al_3^- and Al_3 geometries with the ones reported by Zhan et al. at the CCSD(T)/aug-cc-pVTZ level and found excellent agreement with differences of less than 1 pm in the bond lengths. To further study the effect of the basis set, we then optimized Al_3^- and Al_3 and calculated the ADE with the larger Roos augmented double zeta ANO basis set (DZANO)[38] finding a better value of 1.71 eV, which is closer, but it is still deviated from the experimental value. Our calculated ground state of Al_3 corresponds to a doublet state D_{3h} ($^2A'$) in agreement with the study of Zhan et al.[36] Additionally, Zhan et al. predicted at the CBS level a C_{2v} ($^4A_2$) state 0.29 eV higher in energy than the $^2A'$ ground state. However, Pettersson et al.[39] at the contracted CI (CCI + Q) level predicted the $^4A_2$ state to be ~0.01 eV lower in energy than the $^2A'$ state making them almost degenerate. Interestingly, while magnetic deflection measurements of Al_3 predicted a doublet ground state,[40] earlier electron spin resonance measurements of matrix-insolated Al_3 indicated a quartet ground state.[41] On the basis of these results, we believe that an accurate description of the electron correlation of the system is needed for a precise calculation of the VDE and ADE of Al_3.

Finally, we correctly predicted the ground-state spin multiplicity of the Bi atom as a quartet, and its electron affinity was calculated to be 0.85 eV, which is in good agreement with the experimental value of 0.9424 eV.[23] The molecular geometries and orbitals were plotted using the Schakal[42] and Molden[43] software, respectively.

3. Results and Discussion

Photoelectron spectra of Al_nBi^- ($n = 1-5$) taken at 308 nm are presented in Figure 1 on a binding energy scale. The electron binding energies of anionic clusters deduced by photodetachment correspond to the electron affinities of the neutral clusters. The spectrum of an anionic cluster that has a closed electronic shell is predicted to display a dominant peak that corresponds to a doublet neutral state formed via a one-electron detachment channel. The spectrum of an open-shell cluster anion, corresponding to a doublet state, may show two dominant peaks because of singlet and triplet final states in the neutral species. The anionic ground states of Al_nBi clusters with an odd number of electrons were calculated to be doublet states; this was further confirmed by the observation of two peaks in the experimental spectra of $AlBi^-$ and Al_3Bi^-. The energies of the features are an indicator of the HOMO−LUMO gap of the neutral species in the anionic geometry. The ground states of Al_2Bi^- and Al_4Bi^-, on the other hand, are singlet states, and a single peak was predicted in their experimental spectrum. The higher energy peaks observed for these clusters correspond to removal of electrons from deeper states and may not be accurately described within the current density functional framework. Also, it is important to note that in some cases the resolution of our instrument was not high enough to see individual features as in the spectrum for Al_5Bi^-.

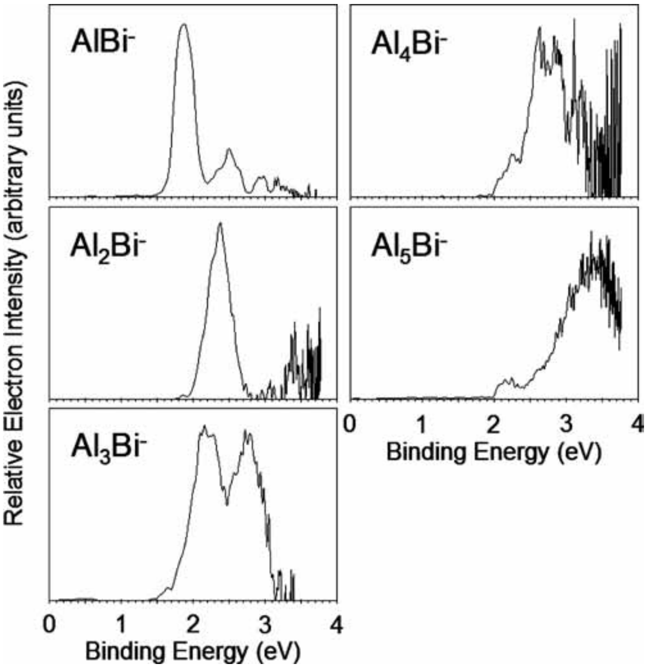

Figure 1. Photoelectron spectra at 308 nm for Al_nBi^- clusters (n = 1−5).

The experimental determination of the vertical detachment energy (VDE) is straightforward as each one corresponds to a band maximum. Additionally, one quantity that can also be observed is the adiabatic detachment energy (ADE), which is taken from the leading edge of the feature in the photodetachment spectrum. These measurements correspond to the difference in energy between the ground state of the anion and the ground state of the neutral species. Table 1 compares the theoretical VDE and ADE with the experimental values. In the case of Al_4Bi^- and Al_5Bi^-, we have also included the VDE calculated for their respective lowest energy lying isomers, which account for the weak peaks at low binding energy (~2 eV) observed in the spectra. As discussed below, for Al_4Bi, the calculated ground-state geometries of the neutral and anionic forms were very different. Thus, the observed ADE is attributed to a transition from the Al_4Bi^- C_2 (^1A) ground state to the lowest energy isomer of the neutral Al_4Bi C_{2v} ($^2A_1$) state. For both Al_4Bi^- and Al_5Bi^-, the low-energy-lying isomers are predicted to be less than 0.27 eV higher in energy than the ground state implying that under the experimental conditions employed, these states are accessed. Additionally, the VDE determination for Al_5Bi^- is attributed to the maximum of the shoulder feature, located at 2.60 eV, whose assumed width is equal to the instrumental resolution at this electron energy (about 700 meV). This shoulder is a separate, reproducible feature from the larger peak located around 3.35 eV.

We have also listed in Table 1 the calculated adiabatic ionization potential (IP) and the calculated HOMO−LUMO gap

TABLE 1: Experimental and Calculated Adiabatic Detachment Energies (ADE) and Vertical Detachment Energies (VDE) of Al_nBi^- ($n = 1-5$) Clusters and Calculated Adiabatic Ionization Potentials (IP) and HOMO−LUMO Gap Values for the Ground-State Al_nBi ($n = 1-6$) Clusters[c]

#Al atoms	E_{rel}	ADE (exptl)	ADE (theor)	VDE (exptl)	VDE (theor)	IP (theor)	HOMO−LUMO gap (theor)
1		1.59 ± 0.07	1.94	1.90, 2.50	1.97, 2.70	6.75	0.46
2		1.97 ± 0.05	2.06	2.37	2.32	7.04	0.72
3	0.0	1.62 ± 0.07	1.72	2.10, 2.68	1.95, 2.78	7.08	1.69
4	0.0	2.36 ± 0.10[a]	2.19 (2.29[b])	2.60[a]	2.42	6.19	0.57
	0.25			2.23	2.16		
5	0.0	2.32 ± 0.10[a]	2.17	2.60[a]	2.59, 2.60	6.51	1.15
	0.27			2.15, 2.60	2.22, 2.57		
6			2.21			6.04	0.51

[a] ADE and VDE from the larger features in the photoelectron spectra corresponding to the ground state. [b] ADE calculated from the ground-state Al_4Bi^- to the lowest energy isomer of Al_4Bi (see the text for details). [c] The calculated relative energies and ADE are also given for the lowest energy lying isomers of Al_nBi^- ($n = 4-5$). All values are in units of eV.

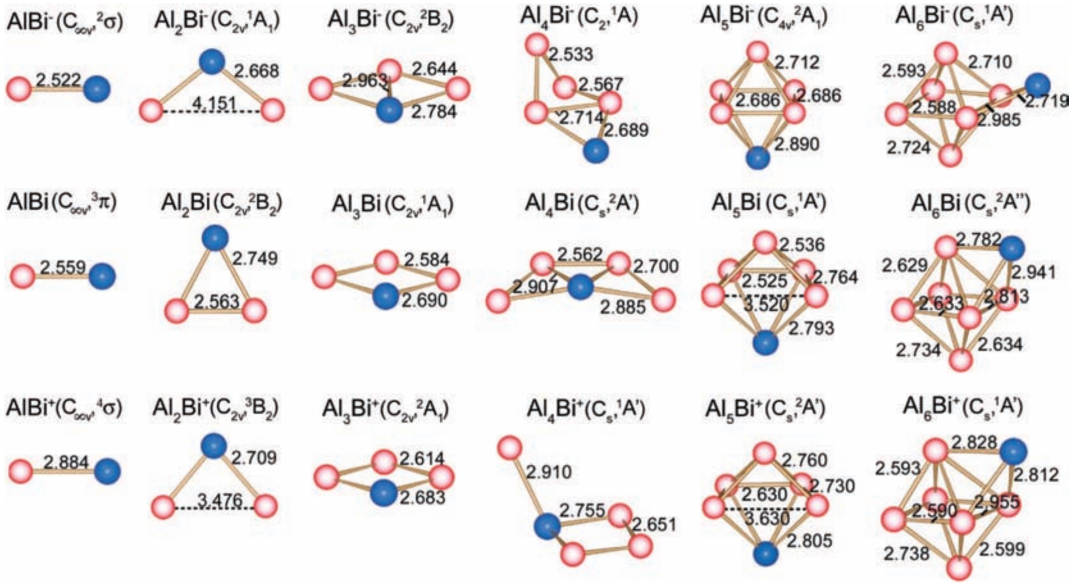

Figure 2. Optimized geometries of anionic, neutral, and cationic Al_nBi clusters ($n = 1-6$). Symmetry point group and electronic state are given in parenthesis. Bond lengths are given in angstroms.

of the neutral species. The calculated gap for the clusters that have an odd number of electrons represents the difference in energy between the singly occupied upper valence orbital and the lowest unoccupied level in the opposing spin manifold. If one includes the uncertainty in experimental measurements, the calculated VDE and ADE are in very good agreement with the experimental values with a maximum difference of 15% for the ADE of AlBi. For Al_3Bi, the experimental value of 1.62 ± 0.07 eV for the ADE agrees well with the calculated value of 1.72 eV.

The photodetachment spectrum of Al_3Bi^- (Figure 1) shows two broad peaks corresponding, respectively, to transitions to the singlet (pictured in Figure 2 as (C_{2v}, $^1A_1$)) and triplet (calculated to be (C_s, $^3A'$)) neutral states. The peaks are located around 2.10 and 2.68 eV in the spectrum in reasonable agreement with the calculated values of 1.95 and 2.78 eV. Theoretical evidence of the stability of Al_3Bi and Al_5Bi emerges from the analysis of the HOMO−LUMO gap, ADE, and IP of the Al_nBi series reported in Table 1. Al_3Bi and Al_5Bi simultaneously possess the larger HOMO−LUMO gaps, the lower ADE, and a higher IP when compared to neighboring sizes.

Figure 2 shows the calculated ground-state geometries, symmetry point group, and electronic state of the anionic, neutral, and cationic Al_nBi ($n = 1-6$) clusters. Figure 3 shows the calculated geometries of the ground states and lowest energy lying isomers for Al_3Bi^-, Al_4Bi^-, Al_5Bi^-, and Al_4Bi. For Al_4Bi, three low-energy-lying isomers were found around 0.09 eV higher than the ground state with the lowest lying energy isomer C_{2v} ($^2A_1$) found to be more similar to the anionic Al_4Bi^- cluster.

The primary focus of the theoretical study was to examine the electronic structure and stability of neutral Al_3Bi, which we suspected would show signs of aromaticity. The ground state of neutral Al_3Bi was indeed found to have a planar C_{2v} ($^1A_1$) structure. Being aromatic, the lowest energy nonplanar state of Al_3Bi was expected to be substantially higher in energy compared to the planar ground state. This was indeed found to be the case as a C_{3v} ($^1A_1$) state was found to be 0.98 eV higher in energy.

Before we proceed further, we would like to add that previous studies exist on systems similar to the Al_3Bi cluster, and we consider it relevant to compare the behavior of Al_3Bi with these systems. Guo and Wu reported the low-lying structures of Al_3P both at the LSDA and B3LYP levels using the 6−311+G(d) basis set.[44] The B3LYP calculations predicted for the lowest energy structure a D_{3h} ($^1A'$) state where the P atom occupies an internal position of a triangle formed by the Al atoms, while a distorted rhombus structure, C_{2v} ($^1A_1$), was 0.37 higher in energy. It was, however, noted by Guo and Wu that the order of the isomers was reversed in the LSDA calculations with the C_{2v} ($^1A_1$) structure being 0.28 eV lower in energy than the D_{3h} ($^1A'$) state. The low-lying electronic states of neutral and anionic Al_3As were investigated by Archibong and St-Amant[16] at the

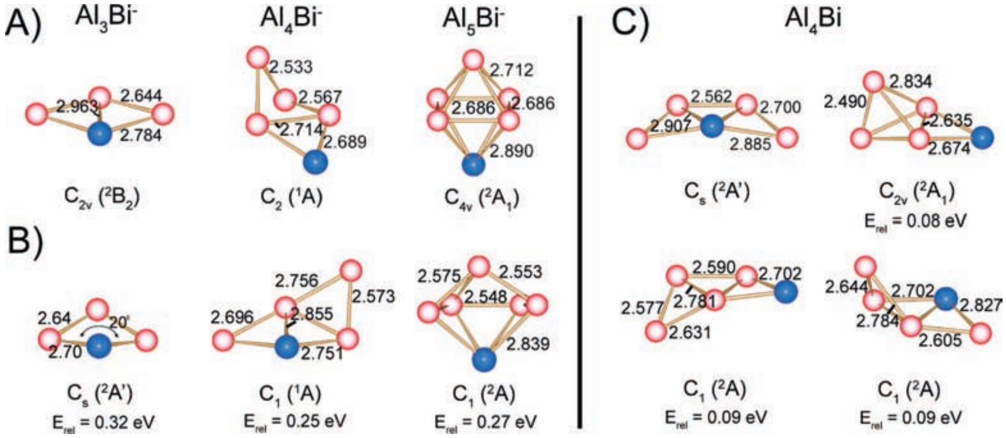

Figure 3. Optimized geometries of the ground state (A) and lowest energy lying isomer (B) of the anionic Al_nBi^- clusters ($n = 3-5$). Optimized geometries of the ground state and lowest energy lying isomers of the neutral Al_4Bi cluster (C). Symmetry point group and electronic state in parentheses are given. Bond lengths are given in angstroms, and relative energies (E_{rel}) are given in units of eV.

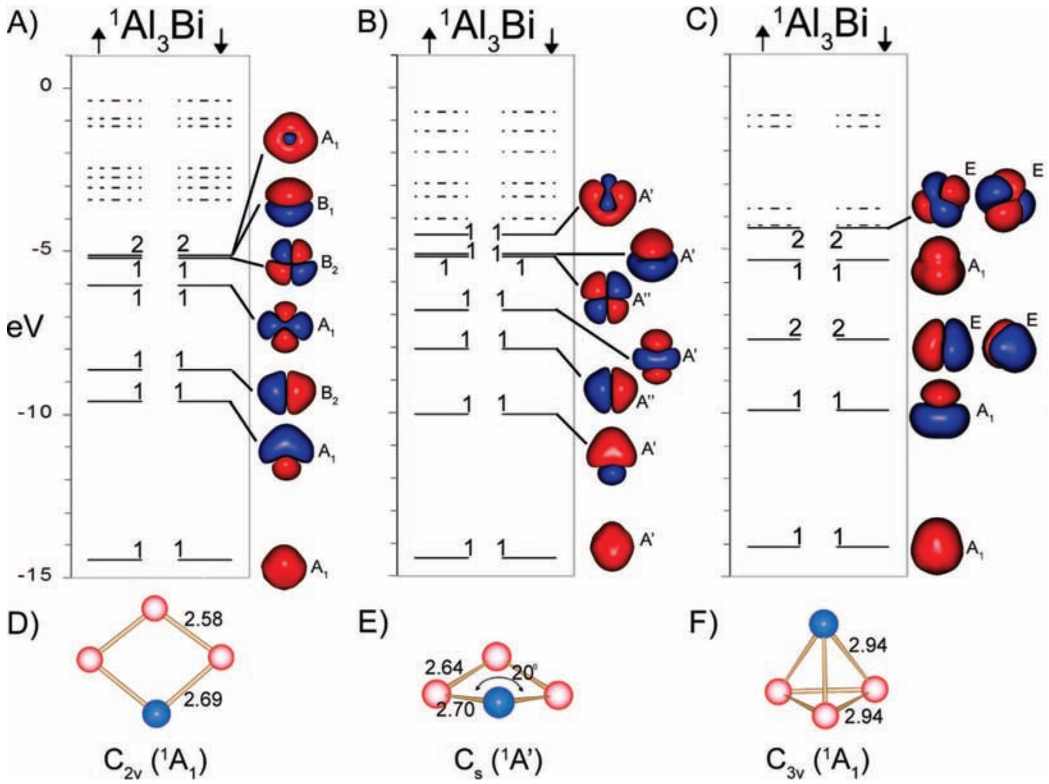

Figure 4. One-electron levels, isosurfaces (isovalue = 0.001 au) and symmetries of the molecular orbitals, and optimized geometries for the 14-electron Al_3Bi cluster at the neutral ground-state geometry (panels A and D), at the C_s anion lowest lying energy isomer geometry (panels B and E), and at the compact C_{3v} geometry (panels C and F). The superscripts indicate spin multiplicity. The continuous lines represent occupied levels, the dotted lines correspond to single unfilled states, the degeneracy is marked next to each level, and the arrows indicate the majority (up) and minority (down) spin states. Bond lengths are given in angstroms.

B3LYP and CCSD(T) levels using the 6−311+G(2df) basis set, and with the same basis set, Guo and Wu[45] reported the ground states of neutral and anionic Al_3As using pure and hybrid exchange correlation functionals. Both studies reported a planar C_{2v} ($^1A_1$) ground state for Al_3As, and additionally, Archibong and St-Amant reported a C_{3v} ($^1A_1$) state 0.17 eV higher in energy at the CCSD(T) level. To compare our method with these previous studies, we performed additional calculations of the Al_3P, Al_3As, and Al_3Sb neutral clusters at the PBE96/DZVP level. For all these systems, we found that the ground state corresponds to a planar C_{2v} ($^1A_1$) structure in analogy to Al_3Bi. In the case of Al_3P, we found a D_{3h} ($^1A'$) state 0.17 eV higher in energy, while for Al_3P, Al_3As, and Al_3Sb, a C_{3v} ($^1A_1$) state was found, respectively, to be 0.27, 0.41, and 0.76 eV higher in energy. These studies will be reported in a coming paper, which will also include experimental work on the Al_nAs and Al_nSb systems.

Coming back to Al_3Bi, we find that the molecular orbital energies in the ground-state planar C_{2v} ($^1A_1$) structure showed a large HOMO−LUMO gap of 1.69 eV. To further probe its bonding character, we investigated the nature of the molecular orbitals. A molecular orbital analysis of Al_3Bi (Figure 4) attests to its aromatic makeup. Figure 4A shows that the three most energetic occupied orbitals, the (A_1) HOMO, (B_1) HOMO-1, and (B_2) HOMO-2, are all delocalized. The HOMO has σ delocalization from the $p_{x,y}$ atomic orbitals oriented radially toward the center of the ring. The electron density lies in the center of the Al_3Bi ring and around the perimeter. The HOMO-1 is a delocalized π orbital from the atomic p_z orbitals perpendicular to the plane of the ring, which results in electron density delocalization above and below the ring similar to benzene. The third delocalized orbital, HOMO-2, is of the σ-type caused by overlap between the atomic $p_{x,y}$ orbitals oriented tangentially around the ring. In this orbital, the two electrons are delocalized between the atoms in the heterocyclic unit. These electronic sequences are similar to those found for Al_4^{2-} and other all-metal, aromatic tetramer anions.[10,12,13] There are, however, slight distortions in the symmetry of Al_3Bi when compared to the delocalized orbitals for the more symmetric Al_4^{2-}, but since the Pauling electronegativity difference between bismuth (1.9) and aluminum (1.5) is small,[46] the extent of delocalization in Al_3Bi is still substantial. This can be seen from a vantage point above the ring in the HOMO-1 (Supporting Information, Figure S1).

Aromatic stability is linked to the filling of molecular σ and π orbitals and should be destroyed if any additional electrons are present. A study of the electronic structure of the Al_3Bi^- anion demonstrates this. Figure 2 shows that anionic Al_3Bi^- in a C_{2v} ($^2B_2$) state has a planar ground-state structure like Al_3Bi. This result is consistent with the studies of Archibong and St-Amant[16] and Guo and Wu[45] who reported for the analogous Al_3As^- cluster a similar C_{2v} ($^2B_2$) ground state. Interestingly, Archibong and St-Amant also predicted a nonplanar C_s ($^2A'$) state 0.59 eV higher in energy than the ground state. In our case, for the Al_3Bi^- anion, we found a nonplanar C_s ($^2A'$) state 0.32 eV higher in energy than the ground state (Figure 3). Preliminary calculations of the anionic Al_3P^-, Al_3As^-, and Al_3Sb^- clusters found a C_{2v} ($^2B_2$) ground state and a nonplanar C_s ($^2A'$) state ~0.36 eV higher in energy for all these anionic clusters.

On the basis of these results, one concludes that adding an electron to the aromatic Al_3Bi cluster reduces the difference in energy between the planar and compact configurations, that is, from 0.98 eV in neutral Al_3Bi to only 0.32 eV in the anion Al_3Bi^-. To further investigate how the geometric distortion affects the electronic structure, we plot in Figure 4B the one-electron levels and molecular orbitals of Al_3Bi in the nonplanar anion Al_3Bi^- structure. The most apparent difference in the electron levels in the nonplanar geometry is the destabilization of the highest occupied delocalized σ orbital. In the planar geometry, this orbital has A_1 symmetry and is degenerate with the π HOMO of B_1 symmetry as seen in Figure 4A. When the geometry is altered in Figure 4B, the π molecular orbital is converted to the HOMO-1 with A′ symmetry and is substantially lower in energy than the HOMO. Furthermore, the calculated HOMO−LUMO gap of the neutral species in the nonplanar geometry is reduced to 0.52 eV (from 1.69 eV in the planar configuration). The calculated HOMO−LUMO gap of the neutral species in the anion planar ground-state geometry is also reduced to 0.95 eV.

To examine the effects of geometry on the electronic structure of Al_3Bi further, the planar ground-state structure was forced into a theoretical compact geometry. Figure 4C shows the one-electron levels and molecular orbitals of Al_3Bi in a pyramidal C_{3v} geometry. In this compact structure, the seven orbitals (14 electrons) rearrange themselves into an electronic structure that roughly resembles the energy levels and geometries within an open-shell Jellium framework. As 18 electrons are needed for a shell closing, the addition of 4 more electrons to the system would satisfy a complete Jellium configuration. The molecular orbital diagram, shown in Figure 4C, depicts both the occupied and unoccupied levels of the pyramidal Al_3Bi. The LUMO is almost degenerate with the HOMO, and the addition of four electrons would occupy the LUMO and LUMO + 1 levels. In the 14 electron system shown, the energy gap between the LUMO + 1 and the LUMO + 2 is greater than 2 eV. It is reasonable to assume that if the LUMO and LUMO + 1 in Figure 4C were filled, an Al_3Bi cluster with C_{3v} geometry and 18 electrons could be stable within a Jellium framework.

We have shown how the addition of electrons to Al_3Bi can drive the cluster system away from aromatic stability and toward Jellium stability. In Al_3Bi, the six electrons occupying the p-states lead to the aromatic stability shown in Figure 4A. Furthermore, the inner-core states are well-separated in energy from the three levels nearest to the delocalized orbitals. With the separation between deeper s-states and the upper valence manifold in mind, we added two extra electrons to the neutral Al_3Bi cluster in order to examine if the set of eight uppermost electrons would lead to a stable cluster within the Jellium scheme that has a large HOMO−LUMO gap. The examination of the electronic and geometric structures would then indicate the mechanisms for stabilization similar to the study of Al_3Bi in a pyramidal geometry above. Figure 5 shows the evolution of the one-electron levels, molecular orbitals, and ground-state geometries of the neutral, anion, and dianion forms of the Al_3Bi cluster. With each electron that is added to the neutral cluster, rearrangement/reordering of the electronic energy levels occurs as would be expected for a system moving away from aromatic stability and toward Jellium stability. In Figure 5A, the (B_1) HOMO-1 in the neutral Al_3Bi, responsible for π aromaticity, is energetically degenerate with the (A_1) HOMO. Figure 5B shows that the (B_1) HOMO-1 orbital in Al_3Bi is displaced in Al_3Bi^-, where it becomes the (B_1) HOMO-3. There is at least 1.0 eV separating this π orbital from the HOMO in Al_3Bi^-. Since the displaced orbital is lower in energy, it is expected to contribute less to the overall valence makeup of the anionic cluster. Adding a second electron further displaces this orbital, which now becomes the (B_1) HOMO-3 in Figure 5C. In the dianion, the difference in energy between the (B_2) HOMO and (B_1) HOMO-3 is well over 1 eV. These results show that just adding electrons to Al_3Bi is not enough to achieve a Jellium-like electronic shell structure. First, the HOMO−LUMO gap in Al_3Bi^{2-} is only 0.73 eV, which is not a large value when compared to the calculated HOMO−LUMO gap of a cluster with true Jellium stability, such as Al_{13}^- (1.87 eV).[47] Second, the geometry of the Al_3Bi^{2-} dianion is planar as seen in Figure 5F. The two-dimensional geometry is a result of the Coulomb repulsion between the extra electrons, and the molecular geometry of Al_3Bi^{2-} is at odds with the requisite Jellium compact geometry. As a consequence, there is a less-than-expected increase in the HOMO−LUMO gap, and the molecular orbitals of Al_3Bi^{2-} do not approach the electronic structure predicted by the Jellium model.[48]

To overcome the Coulomb repulsion between extra charges, we undertook a different approach. The mechanisms of stability for Al_3Bi^{2-} in a compact geometry were investigated by adding alkali metal atoms to the cluster. The role of each additional alkali atom was to donate the requisite electrons without modifying the overall charge. To this effect, we studied the isoelectronic 16-electron Al_3BiNa^- and Al_3BiNa_2 clusters in which each Na atom is expected to contribute an electron to the upper manifold because of its low ionization potential. The results are shown in Figure 6, which presents the one-electron levels, molecular orbitals, and ground-state geometries of the Al_3Bi, Al_3BiNa^-, and Al_3BiNa_2 clusters. Interestingly, in the Al_3BiNa^- cluster, the Na atom is above the plane in the ground-state structure, and the Al_3Bi plane becomes bent as shown in

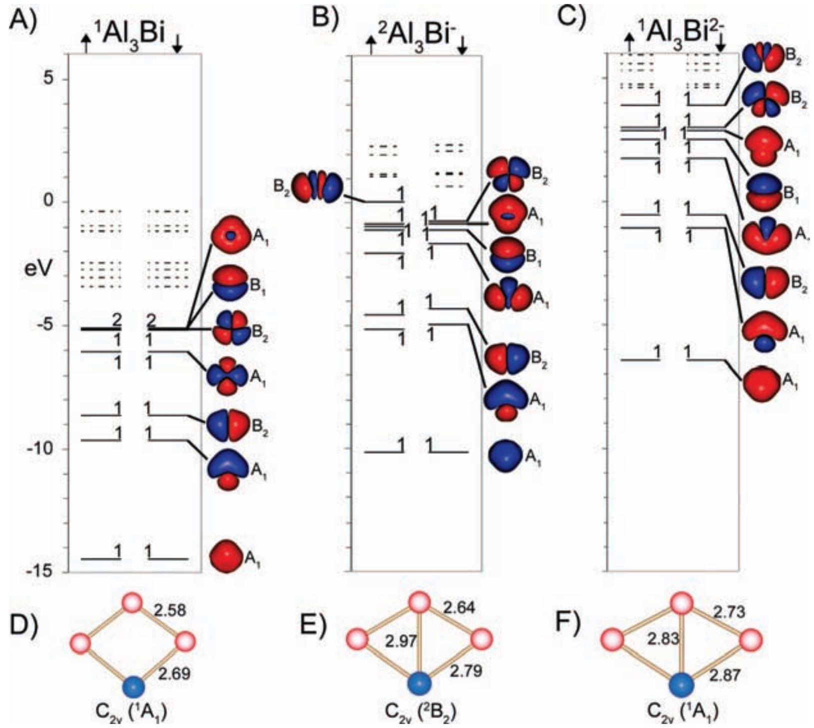

Figure 5. One-electron levels, isosurfaces and symmetry of the molecular orbitals, and optimized geometries for the Al_3Bi cluster (panels A and D), for the Al_3Bi^- cluster anion (panels B and E), and for the Al_3Bi^{2-} cluster dianion (panels C and F). (See caption of Figure 4 for further details.)

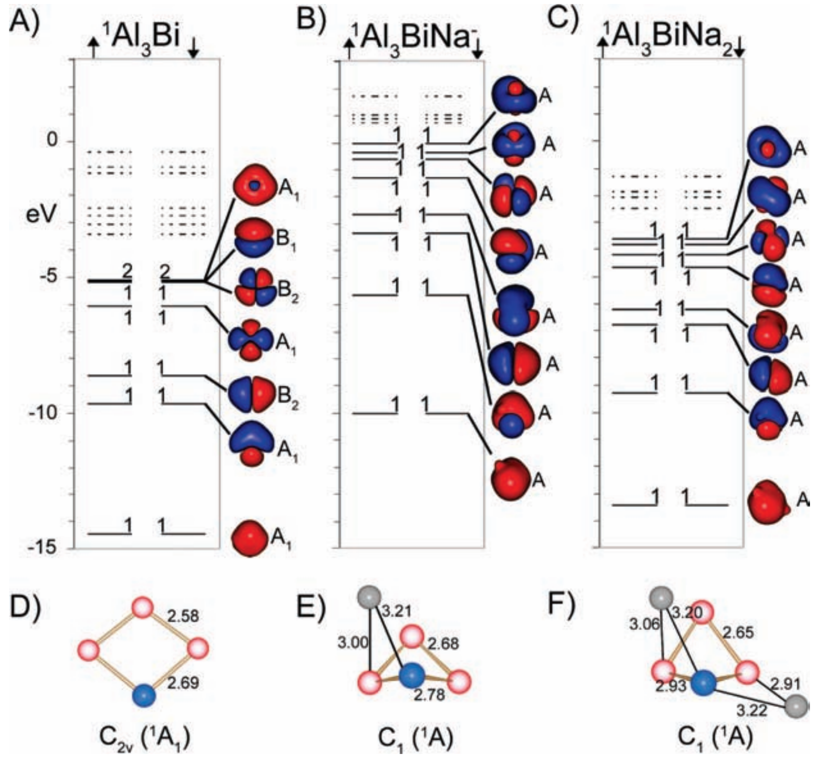

Figure 6. One-electron levels, isosurfaces and symmetries of the molecular orbitals, and optimized geometries for the Al_3Bi cluster (panels A and D), for the anionic Al_3BiNa^- cluster (panels B and E), and for the Al_3BiNa_2 cluster (panels C and F). (See caption of Figure 4 for further details.)

Figure 6E. Because of this condensed geometry, the molecular orbitals rearrange dramatically to produce orbitals beginning to resemble a three-dimensional electron gas seen in Figure 6B. The resulting HOMO−LUMO gap for the anion is 0.78 eV, which is larger than the gap for Al_3Bi^{2-} (0.73 eV). Since the electron count is the same for both Al_3Bi^{2-} and Al_3BiNa^-, the enhancement in stability of the latter can be attributed to its compact geometry. The addition of another Na to form Al_3BiNa_2 further deforms the structure, shown in Figure 6F, with one Na atom above the heterocyclic Al_3Bi unit and the other on top of an Al−Bi bond. In Figure 6C, it is clear that the valence molecular orbitals are more delocalized in Al_3BiNa_2 than those in Al_3Bi^{2-} (Figure 5C). Contrary to Al_3Bi^{2-}, the four uppermost doubly occupied energy levels in Al_3BiNa_2 group together to accommodate eight electrons and, in turn, enhance the stability of the 16-electron cluster. This is evinced by a large HOMO−LUMO gap of 1.12 eV. From these findings, we deduce that the mechanisms for a cluster to approach Jellium stabilization will only occur with a proper electron count and a compact geometry, while aromatic stabilization in these small clusters will only occur with a proper electron count and planar geometry.

An independent signature of aromatic behavior is the nucleus-independent chemical shift (NICS) proposed by Schleyer and Jiao.[49] It provides a magnetic criterion to mirror the ring current and, hence, to identify aromaticity. Systems with negative NICS values tend to be aromatic, while systems with positive NICS values may be classified as antiaromatic. We calculated the NICS values using the same theoretical model in the Gaussian 03 program,[50] that is, the PBE96 functional,[25] DZVP basis set for Al,[27] and a 23 electron scalar relativistic effective core potential[28] with aug-cc-pVDZ[29] basis set for Bi. We found that Al_3Bi gives rise to a large, negative NICS value at the center of the ring (−32.19 ppm), and this value increased as we calculated the NICS value above the plane again affirming the aromatic character. This was also true for the charged clusters Al_3Bi^- and Al_3Bi^+, although the neutral had the most negative NICS value. These results are presented in Table S3 of the Supporting Information.

To further emphasize the correlation between Al_3Bi and Al_4^{2-}, we examined the vibrational modes of alkali metal interactions. The clusters Al_4Li^- and Al_4Li_2 have been previously found to exhibit floppy modes because of the large fluxionality of the Li atoms.[51] These modes lead to low vibrational frequencies for Al_4Li^- and Al_4Li_2 of 96 and 63 cm^{-1}, respectively, corresponding to movement of the lithium atoms. For Al_4Li^-, the frequency of 96 cm^{-1} represents the Li atom hopping to the corners and back to the position on top of the ring center, and in Al_4Li_2, the vibrational frequency of 63 cm^{-1} is a consequence of the collective motions between Li atoms. In our case, we also found vibrational frequencies of 40.3 and 27.9 cm^{-1} corresponding to the movement of the Na atoms in Al_3BiNa^- and Al_3BiNa_2, respectively, indicating a comparable fluxional nature in these clusters.

Figure 7 shows the molecular orbitals and one-electron levels for Al_5Bi, which has a suitable geometry and electron count for a completely filled shell described by the Jellium model. The orbitals are consistent with what is expected for a 20-electron cluster that exhibits Jellium stabilization, which ideally presents a $1s^2$, $1p^6$, $1d^{10}$, and $2s^2$ electronic configuration. As mentioned above for Al_3Bi in a hypothetical C_{3v} symmetry, the lowest energy occupied orbital (A′) in Al_5Bi represents the Jellium $1s^2$ level, and the next three levels make up the Jellium $1p^6$. The $1d^{10}$ and $2s^2$ levels in Al_5Bi are mixed, but there are enough electrons to fully occupy both states. Of the six upper-valence orbitals, the (A′) HOMO-3 in Figure 7 has the most character from the Jellium $2s^2$ level. This is implicit from its distorted spherical shape. The rest of the six upper valence orbitals have the most d-character. As shown in Figure 2, the structure is three-dimensional and compact meeting the requirement for Jellium stability. The electron count (20) combined with a compact, three-dimensional geometry makes the stable Al_5Bi a possible superatom candidate.

As an added test for the stability of Al_3Bi and Al_5Bi, we examined the energetics of formation for Al_nBi clusters. One method employed was to examine the gain in energy as successive Al atoms are added to a Bi atom, (ΔE_{Al}). Another method was to calculate the binding energy of a Bi atom to Al_n ($n = 1-6$) clusters (ΔE_{Bi}). The results of these investigations are reported in Figure 8. In both cases, Al_3Bi and Al_5Bi emerge as uniquely stable. Considering the energy gains from Al atom addition, there are large values for the formation of Al_3Bi and Al_5Bi from their preceding sizes and only small gains in energy in growing to the next size. Additionally, it is shown in Figure 8 that a Bi atom binds more strongly to Al_3 and Al_5, indicating the enhanced stability of these particular mixed clusters.

The present study demonstrates the delicate relationship between the electron count and the molecular geometry in stable cluster systems. Our pointers of stability include electron detachment energies, ionization potentials, HOMO−LUMO gaps, and formation energies. Within a Jellium picture, it has been shown that clusters with both exactly the number of electrons needed to fill the electronic shells and a condensed geometry are extremely stable and chemically inert. Clusters that have stability described by the Jellium model may be regarded as superatoms resembling atoms of the periodic table. The inclusion of aromaticity as a free-electron gas-stabilizing

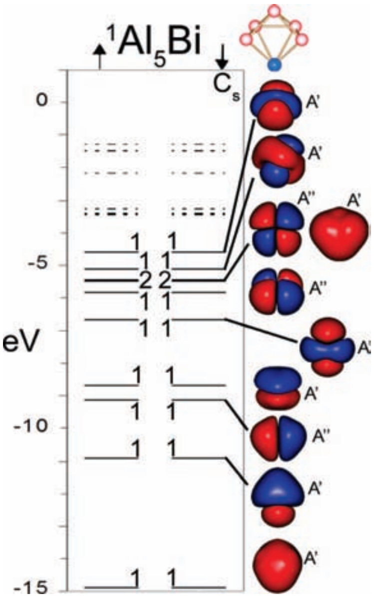

Figure 7. One-electron levels and isosurfaces and symmetries of the molecular orbitals for the 20-electron Al_5Bi cluster. (See caption of Figure 4 for further details.)

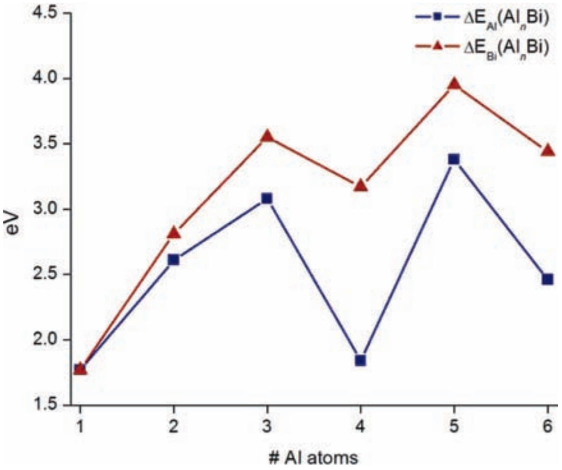

Figure 8. Calculated removal energies (in eV) for aluminum (ΔE_{Al}) and bismuth (ΔE_{Bi}) from the neutral Al_nBi clusters.

force suggests that parallels may be drawn between the two mechanisms. Aside from the more conventional Jellium shell closings (2, 8, 18, 20, ...), occurring with compact geometries, additional shell closings exist for planar arrangements (i.e., 2, 6, 10, 14, ...) that can be described with aromaticity. It is intriguing that there is an all-metal system, namely, Bi doped Al clusters, in which the atoms can combine to form an aromatic, inert species (Al_3Bi) at one size and a filled-shell Jellium cluster (Al_5Bi) at another size. While superatoms have demonstrated their use toward becoming building blocks in a new type of chemistry, all-metal aromatic clusters should be included as another important constituent.

4. Conclusions

The combination of anion photoelectron spectroscopy and theoretical computations has allowed the study of bismuth-doped aluminum clusters. Among the Al_nBi series, lower adiabatic electron detachment energies and calculated higher ionization potentials were obtained for both Al_3Bi, an all-metal aromatic cluster, and Al_5Bi, a Jellium superatom candidate. Theoretical calculations also indicate that they have large HOMO−LUMO gaps, a further testament to their unique stability, and give insight into how electron shell counts and closings work synergistically with geometry. We have shown that the planar Al_3Bi and the three-dimensional, compact Al_5Bi exhibit the type of stability that can be exploited in the synthesis of cluster-based materials.

Benzene is well-known for its ability to form sandwich complexes $M(C_6H_6)_2$, and we believe the planar Al_3Bi might behave in a similar fashion. We also envision the capabilities of forming three-dimensional metal clusters that display unique properties derived from aromatic behavior. It would be interesting to study the reactivity of Al_3Bi similar to the studies performed on other small mixed-metal clusters.[52] A neutral all-metal aromatic species may retain its geometric and electronic structure when undergoing reactions much like benzene. While the electronic and geometric structure indicates that Al_5Bi is a Jellium cluster, future reactivity studies will be required to demonstrate if it is indeed a superatom. Because of their unique stability, the all-metal aromatic Al_3Bi and the potential superatom Al_5Bi show promise for being stable in the condensed phase. It is hoped that the relationship between different mechanisms for electron stability will lead to the design of materials with novel chemical and magnetic properties.

Acknowledgment. We gratefully acknowledge support from the U.S. AFOSR grant FA9550-07-1-0151 for the experimental phase of the work and the U.S. Department of the Army through a MURI grant W911NF-06-1-0280 for the theoretical studies. Part of the calculations were performed on the computational equipment of DGSCA UNAM (General Direction of Academic Computing Services, National Autonomous University of Mexico), particularly in the supercomputer KanBalam.

Supporting Information Available: Supporting figure with two views of the HOMO-1 isosurface of the Al_3Bi cluster. Supporting tables with calculated and previously reported experimental and theoretical ADE and VDE for the Al_n^- ($n = 2-6$) clusters. Table with the calculated NICS values of cationic, anionic, and neutral Al_3Bi clusters. Ground-state Cartesian coordinates of the anionic, neutral, and cationic Al_nBi series and of the Al_3BiNa^- and Al_3BiNa_2 clusters. Cartesian coordinates of the lowest energy lying isomers of Al_3Bi^-, Al_4Bi^-, Al_5Bi^-, and Al_4Bi clusters. Vibrational frequencies with symmetries for the smaller clusters are also included. This material is available free of charge via the Internet at http://pubs.acs.org.

References and Notes

(1) *Small Particles and Inorganic Clusters*; Andersen, H. H., Ed.; Springer: New York, 1997.

(2) *Quantum Phenomena in Clusters and Nanostructures*; Khanna, S. N., Castleman, A. W., Jr., Eds.; Springer: New York, 2003.

(3) Khanna, S. N.; Castleman, A. W., Jr. In *The Chemical Physics of Solid Surfaces. XII. Atomic Clusters: From Gas Phase to Deposited*; Woodruff, D., Ed.; Elsevier: Amsterdam, The Netherlands, 2007; pp 409−425.

(4) (a) Knight, W. D. *Phys. Rev. Lett.* **1984**, *52* (24), 2141. (b) Ekardt, W. *Phys. Rev. B* **1984**, *29* (4), 1558.

(5) Leuchtnr, R. E.; Harms, A. C.; Castleman, A. W., Jr. *J. Chem. Phys.* **1989**, *91* (4), 2753.

(6) (a) Bergeron, D. E.; Castleman, A. W., Jr.; Morisato, T.; Khanna, S. N. *Science* **2004**, *304* (5667), 84. (b) Bergeron, D. E.; Roach, P. J.; Castleman, A. W., Jr.; Jones, N. O.; Khanna, S. N. *Science* **2005**, *307* (5707), 231.

(7) (a) Reber, A. C.; Khanna, S. N.; Castleman, A. W., Jr. *J. Am. Chem. Soc.* **2007**, *129* (33), 10189. (b) Roach, P. J.; Reber, A. C.; Woodward; Khanna, S. N.; Castleman, A. W., Jr. *Proc. Natl. Acad. Sci.* **2007**, *104* (37), 14565.

(8) Kekulé, A. *Bull. Soc. Chim. Fr. (Paris)* **1865**, *3*, 98.

(9) Garratt, P. J. *Aromaticity*; John Wiley & Sons: New York, 1986.

(10) Li, X.; Kuznetsov, A. E.; Zhang, H. F.; Boldyrev, A. I.; Wang, L.-S. *Science* **2001**, *291* (5505), 859.

(11) Boldyrev, A. I.; Kuznetsov, A. E. *Inorg. Chem.* **2002**, *41* (3), 532.

(12) Kuznetsov, A. E.; Boldyrev, A. I.; Li, X.; Wang, L.-S. *J. Am. Chem. Soc.* **2001**, *123* (36), 8825.

(13) Li, X.; Zhang, H. F.; Wang, L.-S.; Kuznetsov, A. E.; Cannon, N. A.; Boldyrev, A. I. *Angew. Chem., Int. Ed.* **2001**, *40* (10), 1867.

(14) Kuznetsov, A. E.; Boldyrev, A. I. *Struct. Chem.* **2002**, *13* (2), 141.

(15) Zhan, C.-G.; Zheng, F.; Dixon, D. A. *J. Am. Chem. Soc.* **2002**, *124* (49), 14795.

(16) Archibong, E. F.; St-Amant, A. *J. Phys. Chem. A.* **2002**, *106* (32), 7390.

(17) Gómez, H.; Taylor, T. R.; Neumark, D. M. *J. Phys. Chem. A.* **2001**, *105* (28), 6886.

(18) (a) Boldyrev, A. I.; Wang, L.-S. *Chem. Rev.* **2005**, *105* (10), 3716. (b) Zubarev, D. Y.; Averkiev, B. B.; Zhai, H.-J.; Wang, L.-S.; Boldyrev, A. I. *Phys. Chem. Chem. Phys.* **2008**, *10* (2), 257.

(19) Li, X.; Wu, H.; Wang, X.-B.; Wang, L.-S. *Phys. Rev. Lett.* **1998**, *81* (9), 1909.

(20) Reveles, J. U.; Khanna, S. N.; Roach, P. J.; Castleman, A. W., Jr. *Proc. Natl. Acad. Sci.* **2006**, *103* (49), 18405.

(21) Knappenberger, K. L., Jr.; Jones, C. E., Jr.; Sobhy, M. A.; Castleman, A. W., Jr. *Rev. Sci. Instrum.* **2006**, *77* (12), 123901.

(22) Wiley, W. C.; McLaren, I. H. *Rev. Sci. Instrum.* **1955**, *26* (12), 1150.

(23) Andersen, T.; Haugen, H. K.; Hotop, H. *J. Phys. Chem. Ref. Data* **1999**, *28* (6), 1511.

(24) Kohn, W.; Sham, L. J. *Phys. Rev.* **1965**, *140* (4A), A1133.

(25) Perdew, J. P.; Burke, K.; Ernzerhof, M. *Phys. Rev. Lett.* **1996**, *77* (18), 3865.

(26) Köster, A. M.; Calaminici, P.; Casida, M. E.; Flores-Moreno, R.; Geudtner, G.; Goursot, A.; Heine, T.; Ipatov, A.; Janetzko, F.; del Campo, J. M.; Patchkovskii, S.; Reveles, J. U.; Salahub, D. R.; Vela, A. *deMon2k*, V. 2.3.6; The deMon Developers Community: Cinvestav, México, 2006; available at www.deMon-software.com.

(27) Godbout, N.; Salahub, D. R.; Andzelm, J.; Wimmer, E. *Can. J. Chem.* **1992**, *70* (2), 560.

(28) Metz, B.; Stoll, H.; Dolg, M. *J. Chem. Phys.* **2000**, *113* (7), 2563.

(29) Peterson, K. A. *J. Chem. Phys.* **2003**, *119* (21), 11099.

(30) Dunlap, B. I.; Connolly, J. W. D.; Sabin, J. R. *J. Chem. Phys.* **1979**, *71* (12), 4993.

(31) Mintmire, J. W.; Dunlap, B. I. *Phys. Rev. A* **1982**, *25* (1), 88.

(32) Köster, A. M.; Flores-Moreno, R.; Reveles, J. U. *J. Chem. Phys.* **2004**, *121* (2), 681.

(33) Flores-Moreno, R.; Alvarez-Mendez, J.; Vela, A.; Köster, A. M. *J. Comput. Chem.* **2006**, *27* (9), 1009.

(34) Reveles, J. U.; Köster, A. M. *J. Comput. Chem.* **2004**, *25* (9), 1109.

(35) Sun, J.; Lu, W. C.; Wang, H.; Li, Z. S.; Sun, C. C. *J. Phys. Chem. A* **2006**, *110* (8), 2729.

(36) Zhan, C.-G.; Zheng, F.; Dixon, D. A. *J. Am. Chem. Soc.* **2002**, *124*, 14795.

(37) Cha, C.-Y.; Ganteför, G.; Eberhardt, W. *J. Chem. Phys.* **1994**, *100*, 995.

(38) Windmark, P. O.; Persson, B. J.; Ross, B. O. *Theor. Chim. Acta* **1991**, *79*, 419.

(39) Pettersson, L. G. M.; Bauschlicher, C. W.; Halicioglu, T. *J. Chem. Phys.* **1987**, *87*, 2205.

(40) Cox, D. M.; Trevor, D. J.; Whetten, R. L.; Rohlfing, E. A.; Kaldor, A. *J. Chem. Phys.* **1986**, *84*, 4651.

(41) Howard, J. A.; Sutcliffe, R.; Tse, J. S.; Dahmane, H.; Mile, B. *J. Phys. Chem.* **1985**, *89*, 3595.

(42) Keller, E. *Chem. Unserer Zeit* **1980**, *14* (2), 56; available at www.krist.uni-freiburg.de/ki/Mitarbeiter/Keller/schakal.html.

(43) Schaftenaar, G.; Noordik, J. H. *J. Comput.-Aided Mol. Des.* **2000**, *14* (2), 123; available at www.cmbi.ru.nl/molden/molden.html.

(44) Guo, L.; Wu, H. J. *Nanopart. Res.* **2008**, *10*, 341.

(45) Guo, L.; Wu, H.-S. *Eur. Phys. J. D.* **2007**, *42*, 259.

(46) Pauling, L. *The Nature of the Chemical Bond and the Structure of Molecules and Crystals*, 3rd ed.; Cornell University Press: Ithaca, NY, 1960.

(47) Khanna, S. N.; Rao, B. K.; Jena, P. *Phys. Rev. B* **2002**, *65* (12), 125105.

(48) Han, Y.-K.; Jung, J. *J. Am. Chem. Soc.* **2008**, *130* (1), 2.

(49) Schleyer, P. V. R.; Jiao, H. *Pure Appl. Chem.* **1996**, *68* (2), 209.

(50) Frisch, M. J.; Trucks, G. W.; Schlegel, H. B.; Scuseria, G. E.; Robb, M. A.; Cheeseman, J. R.; Montgomery, J. A., Jr.; Vreven, T.; Kudin, K. N.; Burant, J. C.; Millam, J. M.; Iyengar, S. S.; Tomasi, J.; Barone, V.; Mennucci, B.; Cossi, M.; Scalmani, G.; Rega, N.; Petersson, G. A.; Nakatsuji, H.; Hada, M.; Ehara, M.; Toyota, K.; Fukuda, R.; Hasegawa, J.; Ishida, M.; Nakajima, T.; Honda, Y.; Kitao, O.; Nakai, H.; Klene, M.; Li, X.; Knox, J. E.; Hratchian, H. P.; Cross, J. B.; Bakken, V.; Adamo, C.; Jaramillo, J.; Gomperts, R.; Stratmann, R. E.; Yazyev, O.; Austin, A. J.; Cammi, R.; Pomelli, C.; Ochterski, J. W.; Ayala, P. Y.; Morokuma, K.; Voth, G. A.; Salvador, P.; Dannenberg, J. J.; Zakrzewski, V. G.; Dapprich, S.; Daniels, A. D.; Strain, M. C.; Farkas, O.; Malick, D. K.; Rabuck, A. D.; Raghavachari, K.; Foresman, J. B.; Ortiz, J. V.; Cui, Q.; Baboul, A. G.; Clifford, S.; Cioslowski, J.; Stefanov, B. B.; Liu, G.; Liashenko, A.; Piskorz, P.; Komaromi, I.; Martin, R. L.; Fox, D. J.; Keith, T.; Al-Laham, M. A.; Peng, C. Y.; Nanayakkara, A.; Challacombe, M.; Gill, P. M. W.; Johnson, B.; Chen, W.; Wong, M. W.; Gonzalez, C.; Pople, J. A. *GAUSSIAN-03*, Gaussian Inc.: Wallingford, CT, 2004.

(51) Islas, R.; Heine, T.; Merino, G. J. *Chem. Theory Comput.* **2007**, *3* (3), 775.

(52) Neumaier, M.; Weigend, F.; Hampe, O.; Kappes, M. M. *J. Chem. Phys.* **2006**, *125* (10), 104308.

JP804667D